Cell Reports
Physical Science

CellPress
OPEN ACCESS

Article

Organic Photochemistry-Assisted Nanoparticle Segregation on Perovskites

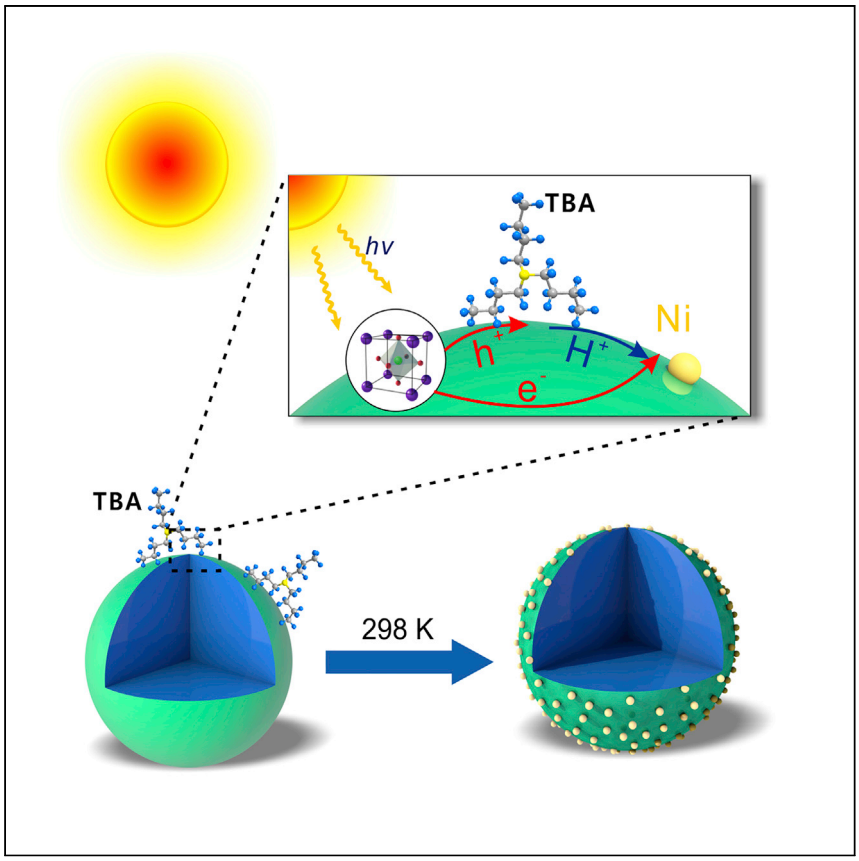

Nanoparticle segregation on perovskite surfaces typically requires high temperature. Here, Chen et al. report trialkyl amine and photo-illumination-assisted surface nanoparticle segregation at room temperature. This strategy may represent an affordable pathway to perovskite functionalization.

Zhou Chen, Bin Hua, Xin Zhang, ..., Zongping Shao, Jing-Li Luo, Yifei Sun

jhli@xmu.edu.cn (J.L.)
yfsun@xmu.edu.cn (Y.S.)

HIGHLIGHTS

Nanoparticle segregation from perovskites at room temperature

Both trialkyl amine and photo-irradiation play pivotal roles in the process

The material functionalized by photoexcitation demonstrates good catalytic activity

Chen et al., Cell Reports Physical Science 1, 100243
November 18, 2020
https://doi.org/10.1016/j.xcrp.2020.100243

Please cite this article in press as: Chen et al., Organic Photochemistry-Assisted Nanoparticle Segregation on Perovskites, Cell Reports Physical Science (2020), https://doi.org/10.1016/j.xcrp.2020.100243

Cell Reports
Physical Science

CellPress
OPEN ACCESS

Article

Organic Photochemistry-Assisted Nanoparticle Segregation on Perovskites

Zhou Chen,[1,5,12] Bin Hua,[2,12] Xin Zhang,[4,12] Lifang Chen,[4] Ya-Qian Zhang,[2] Guangming Yang,[3] Gang Wan,[6] Hua Zhou,[7] Yanling Yang,[5] Jian Chen,[8] Hongqiang Fan,[9] Qian Li,[10] Meng Li,[2] Jianhui Li,[5,*] Wei Zhou,[3] Zongping Shao,[3,11] Jing-Li Luo,[2] and Yifei Sun[1,13,*]

SUMMARY

The segregation (or exsolution) of nanoparticles (NPs) on the surface of perovskite oxide parents has emerged as an advanced technology to design functional materials for renewable energy. However, this process relies heavily upon lengthy reduction (800–1,200 K) in hydrogen-rich environments to facilitate the electron transfer from hydrogen to oxides, making this process costly. Here, we show that, in addition to thermal driving forces, photo-illumination can drive electron donation and facilitate the electron harvesting on perovskite directly. This results in segregation of NPs at room temperature with the assistance of trialkyl amine as a hole acceptor. A proton-coupled electron transfer catalytic cycle is suggested to explain this unusual electron transfer pathway, which is redox neutral and an intrinsically closed cycle. The practicality of this process is demonstrated by the improved performance in a trial electrocatalytic oxygen evolution reaction. This work suggests a promising design principle for perovskite functionalization.

INTRODUCTION

The segregation (or exsolution) of nanoparticles (NPs) covering the perovskite oxide (ABO_3) surface has emerged as an advanced strategy unlocking material functionality for versatile catalytic applications such as fuel cells and water splitting.[1–3] It produces well-confined NPs with tunable composition, transformable morphology, regeneration potential, and superior robustness against coking and coarsening.[4–8] Various catalytic transition metal cations can be incorporated into the B-site of perovskite oxide with even distribution in crystal lattice after annealing in oxygen-rich gas. Nevertheless, in reducing atmosphere, these cations are partially egressed from their B-site hosts and segregate on the surface as NPs with socketed modality. This traditional route is a heterogeneous process in which low partial pressure of oxygen (P_{O2}) and high temperature are essentially required. The enrichment of surface electrons donated by H_2 benefits the yield of numerous metallic NPs, which simultaneously helps the reconfiguration of new stoichiometry.

State-of-the-art structural engineering via phase evolution, non-stoichiometry construction (A-site cation deficiency), and lattice strain control could drastically facilitate cations segregation.[9–11] The electrochemical poling is even able to shorten the timescale of this process by orders of magnitude due to the emergence of transient ultra-low P_{O2}.[12] However, to overcome kinetic restriction of cation diffusion, most cases (including transition metals [e.g., Cu, Ni, Co, Fe, Mn], noble metals [e.g., Pt, Ru, Pd, Rh], and alloy derivates [e.g., Co-Fe, Ni-Fe, Ni-Cu]) still need to

[1]College of Energy, Xiamen University, Xiamen 361005, P.R. China

[2]Department of Chemical and Materials Engineering, University of Alberta, Edmonton, AB T6G 1H9, Canada

[3]Jiangsu National Synergetic Innovation Center for Advanced Materials (SICAM), State Key Laboratory of Materials-Oriented Chemical Engineering, College of Chemical Engineering, Nanjing Tech University, Nanjing 210009, P.R. China

[4]State Key Laboratory of Chemical Resource Engineering, Beijing Advanced Innovation Center for Soft Matter Science and Engineering, Beijing University of Chemical Technology, Beijing 100029, P.R. China

[5]National Engineering Laboratory for Green Chemical Productions of Alcohols-Ethers-Esters, College of Chemistry and Chemical Engineering, Xiamen University, Xiamen 361005, P.R. China

[6]Materials Science Division, Argonne National Laboratory, Lemont, IL 60439, USA

[7]Advanced Photon Source, Argonne National Laboratory, Lemont, IL 60439, USA

[8]Nanotechnology Research Centre, National Research Council Canada, Edmonton, AB T6G 2M9, Canada

[9]Laboratory for Microstructures, Institute of Materials, School of Materials Science and Engineering, Shanghai University, Shanghai 200072, P.R. China

[10]State Key Laboratory of Advanced Special Steels, Shanghai Key Laboratory of Advanced Ferrometallurgy, School of Materials Science and Engineering, and Materials Genome Institute; Shanghai University, Shanghai 200444, P.R. China

[11]Department of Chemical Engineering, Curtin University, Perth, WA 6845, Australia

[12]These authors contributed equally

[13]Lead Contact

*Correspondence: jhli@xmu.edu.cn (J.L.), yfsun@xmu.edu.cn (Y.S.)

https://doi.org/10.1016/j.xcrp.2020.100243

be elicited at high temperature (~900 K), or at least intermediate temperature (600~900 K) for some particular species (e.g., Ag, Ni-Pt) at the expense of a huge amount of thermal-energy input (Figure 1A). Although the "socketed" modality of segregated NPs grants enhanced metal-support interaction and stability,[13] the tension of coarsening/agglomeration due to high temperature is still difficult to completely migrate. The prediction based on Gibbs-free energy indicated that the segregation of metals from oxides (i.e., thermo-driven reduction process) was thermodynamically favorable even at room temperature (Figure S1). However, the H_2-temperature programmed reduction (H_2-TPR) result, which briefly demonstrates the minimum onset temperature of thermo-driven reduction, clearly suggests that it is unrealistic at room temperature (Figure S1). Thereby, it is essentially pivotal to explore other routes targeting efficient surface segregation of NPs under mild condition in terms of energy efficiency and development feasibility.

In organic photochemistry, single electron transfer between an electron acceptor and an electron donor can be triggered under photo-illumination at room temperature, which is conventionally prohibited without photoexcitation.[14] Within such a process, trialkyl amine was highly often used as a single electron reducing reagent.[15] On the other hand, it is noted that many perovskite oxides are semiconductors that can absorb light and drive the formation of photo-excited electrons and holes.[16] Moreover, previous literatures have shown that these photo-generated electrons in semiconductor or transition metal oxides exhibit the potential to reduce themselves to form corresponding metal (as electron acceptor).[17,18] Such a phenomenon could, in turn, provide a new opportunity for the construction of NPs/perovskite architecture in an energy-efficient way. Following this line of thinking, here we demonstrate a readily accessible strategy to initiate NPs segregation on the perovskite surface at room temperature. With the synergistic assistance of trialkyl amine (e.g., tributylamine [TBA]) and photo-illumination, we speculate that an intrinsically closed organic proton-coupled electron transfer (PCET) catalytic cycle effectively leads to the segregation of Ni NPs with a rich population and even distribution (schematic shown in Figure 1B [1–4,9,10,12,13,19–51]).

RESULTS AND DISCUSSION

SFTNi Selection

To exemplify this concept, the Ni and Ti doped the $SrFeO_3$ perovskite with a cubic symmetry: $SrFe_{0.85}Ti_{0.1}Ni_{0.05}O_{3-\delta}$ (SFTNi) was selected. We first utilized density functional theory (DFT) calculations to give an estimated segregation tendency of each element in our material system. The d-band center of the Ni atom is located at −0.32 eV, which is closer to Fermi level than that of the Fe atom at −0.37 eV and that of the Ti atom at −3.31 eV. The estimated values of segregation energy calculated by DFT were −2.76 and −5.23 eV for Ni and Fe from the SFTNi superlattice, respectively. These results suggest that the reduction of Ni ion was much more favorable (Figure S2). Broader exemplification was also shown by the investigation of a series of B-site substituted system ($SrFe_{0.85}Ti_{0.1}M_{0.05}O_{3-\delta}$, where M = Ni, Co, Cu, Pd). We showed that the feasibility of segregation of B-site dopants was closely related to its corresponding d-band center position. The closer the d-band center was to Fermi level, the lower the segregation energy that was required (Figure S3). These findings are consistent with a previous report[19] and our results that only Ni segregation can be found after thermo-driven reduction on SFTNi (Figure S1).

From the perspective of electron transfer, the thermo-driven reduction relied on the electron transfer between H_2 and the perovskite. Differently, the photo-excited

Please cite this article in press as: Chen et al., Organic Photochemistry-Assisted Nanoparticle Segregation on Perovskites, Cell Reports Physical Science (2020), https://doi.org/10.1016/j.xcrp.2020.100243

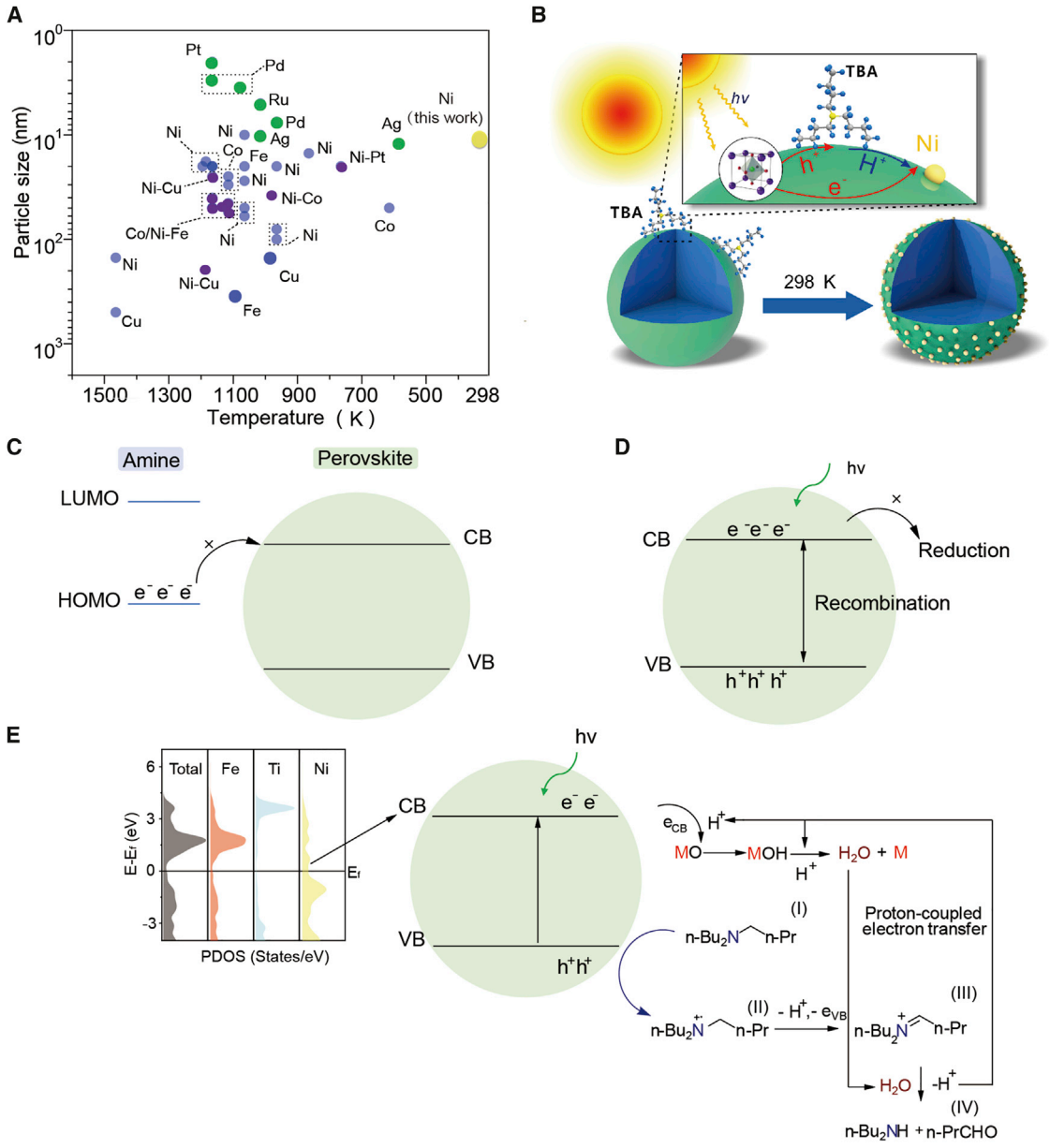

Figure 1. Speculated Mechanism of Photo-Excited Segregation of Nanoparticles on Perovskite Oxide

(A) Summary of segregated NPs parameters (NPs size versus temperature) from representative reports. References were used for Figure 1B.[1–4,9,10,12,13,19–51]

(B) The schematic diagram of photo-excited segregation conception. h^+ and e^- present the hole and electron excited by photo-illumination, respectively. H^+ represents proton. TBA represents tributylamine.

(C) Prohibited electron transfer from amine to the perovskite without illumination. The CB and VB present conduction band and valence band, respectively.

(D) Unfeasible segregation triggered by photo-illumination alone.

(E) The proposed reaction pathway of photo-excited segregation of $SrFe_{0.85}Ti_{0.1}M_{0.05}O_{3-\delta}$. (M = segregated transition metals).

segregation was realized via the photo-induced electron transfer among the organic reductant, solvent, and perovskite. This synergistic effect played an irreplaceable role in photo-excited NPs segregation, and neither TBA nor photo-illumination could realize this process successfully on its own (Figure S4). On one hand, at ground state, the electron transfer from the highest occupied molecular orbital (HOMO) of

TBA to electron acceptor was usually hindered due to its high reduction potential (Figure 1C).[52] On the other hand, under photo-illumination only, the inter-band electron transfer in the perovskite from the hybridized metal$_{3d}$-O$_{2p}$ state near the top of the valence band (VB) to the unoccupied conduction band (CB) of the perovskite was theoretically possible as long as the photon energy is larger than its bandgap.[53] In our system, SFTNi showed an estimated band gap of ~2.0 eV (Figure S5), and the standard reduction potential of SFTNi (0.784 V versus RHE) was much more positive than that of water reduction of 0 V (versus RHE). Thus, the photo-excited electrons prefer to trigger "segregation of Ni"[54] (Note S1; Tables S2–S4). Further, the calculated energy of photo-excited electron was also higher than the reaction enthalpy of NiO_x to Ni^0 (Note S2), further buttressing the theoretical feasibility of Ni segregation by using photo-excited electron. However, the reality is that the recombination of the photo-excited electron-hole pair was usually much faster than the electron transfer in multi-step chemical reactions, which leads to low segregation efficiency (Figure 1D).[55] Therefore, the introduction of an external reducing reagent/electron donor is a promising resolution for efficient photo-excited segregation, since it helps suppress the electron-hole pair recombination and simultaneously facilitates the electron transfer.

An outline of the speculated mechanism for photo-excited segregation with the assistance of trialkyl amine on SFTNi was illustrated in Figure 1E. With the absorption of the photon, the promoted electron with the concomitant hole can be created by interband transitions in the perovskite. The VB bears a more positive potential (~1.9 V versus RHE) than the HOMO of TBA (~0.638–1.638 V versus RHE for alkyl amines).[56] Therefore, the photo-generated hole in the VB oxidized the TBA (I) to the corresponding amine radical cation II, followed by hydrogen radical abstraction by the VB to afford the iminium ion III. With the assistance of reaction from I to II, the photo-generated electron in CB transfers to the active M site with one proton (from II to III) to the product M-OH upon protonation. The generated M-OH was very prone to being reduced through the PCET pathway, the metal was produced in its metallic form (surface segregation), and the stoichiometric H_2O was released. The iminium ion III hydrolyzed with the released H_2O to perfectly close the catalytic cycle. Here, the argon (Ar)-saturated deionized (DI) water was used as a solvent mainly because such polar and protic solvents were generally favored for PCET and suppressed the reversion of PCET.[57] In this practical transformation, the semiconductor material itself serves as a photosensitizer, and its band gap falls in the range of the visible light spectrum. From the universal viewpoint, most of the perovskite oxide candidates obtain an optical bandgap within the solar-light-spectrum range, advocating the potential generality of this method taking advantage of visible light as a driving force.

Morphology illustration of SFTNi after photo-excited segregation (PS-SFTNi) was shown in Figures 2A and 2B. The surface-rich NPs with a smaller average size (~15–25 nm) and even spatial distribution were detected. The study of selected area electron diffraction (SAED) for an individual particle further confirmed the pure metallic nickel nature (Figure 2B). Parallel comparison of different paths illustrated that, as compared to high-temperature H_2 reduction, photo-excited segregation can generate equally high-concentrated and fine NPs with a much more energy-efficient method (Figure S6).

The evolution of surface chemistry of the material during photo-excited segregation was preliminarily analyzed by X-ray photoelectron spectroscopy (XPS). Significant shifts of binding energy peaks of Ni 2p$_{3/2}$ and O 1s spectra were observed on materials treated by H_2-driven and photo-excited segregation, respectively (Figure S7;

Please cite this article in press as: Chen et al., Organic Photochemistry-Assisted Nanoparticle Segregation on Perovskites, Cell Reports Physical Science (2020), https://doi.org/10.1016/j.xcrp.2020.100243

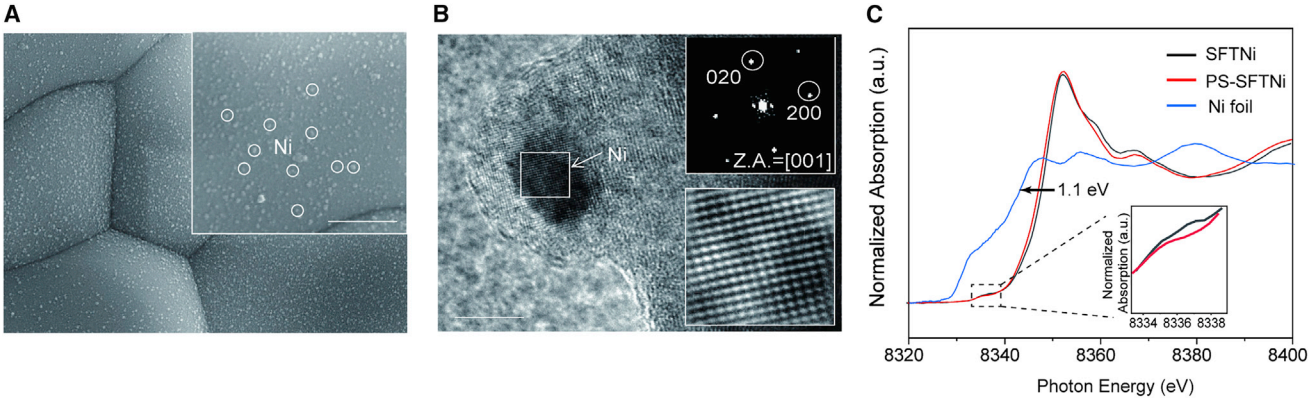

Figure 2. Characterization of NPs by Photo-Excited Segregation

(A) SEM images of PS-SFTNi. The scale bar is 200 nm.

(B) High-resolution TEM image of PS-SFTNi. Selected area electron diffraction (SAED) of an individual Ni particle was shown in inset of Figure 2B. The scale bar is 10 nm.

(C) Ni K-edge X-ray absorption near edge structure (XANES) characterizations of PS-SFTNi, SFTNi, and Ni foil. The zoom-in of pre-edge area is shown in the inset.

Table S1). The Ni K-edge X-ray absorption near-edge structure (XANES) spectra of the SFTNi samples after photo-illumination were further shown in Figure 2C with the reference of Ni foil. The main XANES features of Ni in SFTNi samples were similar to those of octahedra-coordinated Ni(III) in the nickel-doped ferrite perovskite,[58] indicating its high oxidation state. It is confirmed that Ni absorption edge energy dynamically shifted toward to lower values by ~1.1 eV for PS-SFTNi, suggesting the partial nucleation of nickel sites to a lower average oxidation state. Also, the decreased pre-edge area of PS-SFTNi (shown in inset) indicates the change of Ni local symmetry and coordination due to the formation of metallic Ni. With the consideration that the bulk Ni cations have low diffusivity to migrate to the surface and get involved into photo-excited segregation at room temperature, it can be inferred that the Ni cations near the surface should make a major contribution to the NP segregation phenomenon.

OER Probe Reaction

To elucidate the practicability of material after photo-excited segregation, the oxygen evolution reaction (OER) was chosen as the probe reaction. The Ni-based catalysts are promising substitutions for noble metal catalysts due to their high theoretical catalytic activity and low cost.[59,60] The Tafel plot (Figure 3A) for PS-SFTNi revealed a low slope of 85.4 $mV \cdot dec^{-1}$ (millivolt per decade of electrical current density), which was comparable to IrO_2 (83 $mV \cdot dec^{-1}$) and $Ba_{0.5}Sr_{0.5}Co_{0.8}Fe_{0.2}O_{3-c}$ (BSCF) (84 $mV \cdot dec^{-1}$), further stating its more favorable reaction kinetics than SFTNi after H_2 treatment (HE-SFTNi) (101 $mV \cdot dec^{-1}$), and pristine SFTNi (126.6 $mV \cdot dec^{-1}$). The polarization curves for different catalysts shown in Figure 3B demonstrated that the OER onset overpotentials (η) of SFTNi, HE-SFTNi, and PS-SFTNi were at 410, 340, and 290 mV, respectively, suggesting the significant improved performance of SFTNi after the photo-excited segregation. Besides, the value of required overpotentials to achieve a current density of 10 mA cm^{-2} were also measured, which is a metric relevant to solar fuel synthesis.[61] The linear sweep voltammetry (LSV) curve of PS-SFTNi indicated that the operational overpotential of PS-SFTNi was 477 mV, which is superior to the benchmark OER catalyst of BSCF (η = 510 mV) and comparable to IrO_2 (η = 450 mV). Also, this value was much lower than those of HE-SFTNi (η = 558 mV) and pristine SFTNi (η = 650 mV). The mass normalized activity (MA) of

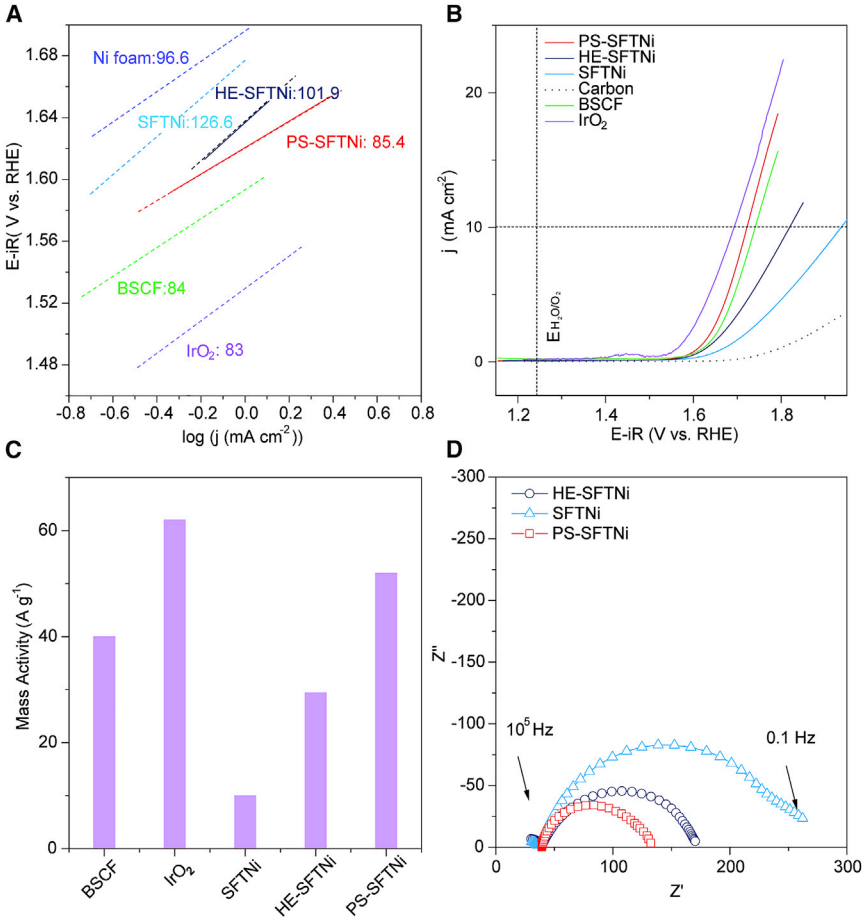

Figure 3. Catalytic Performance Comparison of SFTNi Series Materials

(A) Tafel plots of various catalysts for oxygen evolution reaction (OER).

(B) Linear sweeping voltammogram (LSV) for OER.

(C) Mass normalized activity (MA) at an overpotential of η = 0.5 V for various catalysts.

(D) Electrochemical impedance spectra (EIS) of the SFTNi series electrodes recorded at 1.67 V versus RHE under the influence of an alternating current (AC) voltage of 10 mV.

PS-SFTNi (η = 500 mV) can reach 52 $A \cdot g^{-1}$, which was much higher than those of HE-SFTNi (40 $A \cdot g^{-1}$) and pristine SFTNi (10 $A \cdot g^{-1}$) (Figure 3C). The electrical impedance spectra (EIS) of the samples were also obtained to compare the charge transport process inside the electrodes (Figure 3D). The charge transfer resistance (R_{ct}) of PS-SFTNi (~95 Ω) was smaller than HE-SFTNi (~119 Ω) and pristine SFTNi (~240 Ω), suggesting that PS-SFTNi possessed a facile charge-transfer rate and kinetics due to the exposure of a larger number of active sites.

Enlightened by the PCET catalytic cycle in organic photochemistry, we have shown that the synergetic effect between photo-illumination and photo-organic reductant of trialkyl amine can offer an economic avenue toward the construction of the "NPs/perovskite" heterostructure. Benefitting from this method, the material shows surface decoration of the metal particle with a rich population and better catalytic performance in a probe reaction trial. Beyond that, this approach demonstrates the potential to utilize the combination of intrinsic (bandgap engineering) and extrinsic (organic photochemistry) material-driving forces for the design of the functional perovskite.

Please cite this article in press as: Chen et al., Organic Photochemistry-Assisted Nanoparticle Segregation on Perovskites, Cell Reports Physical Science (2020), https://doi.org/10.1016/j.xcrp.2020.100243

EXPERIMENTAL PROCEDURES

Resource Availability

Lead Contact

Further information and requests for resources and reagents should be directed to and will be fulfilled by the lead contact, Yifei Sun (yfsun@xmu.edu.cn).

Materials Availability

This study did not generate new unique reagents.

Data and Code Availability

The authors declare that the data supporting the findings of this study are available within the article and the Supplemental Information. All other data are available from the lead contact upon reasonable request.

Methods

Detailed experimental sections, figures, tables, and supporting notes are listed in Supplemental Experimental Procedures. Supporting information is available free of charge from the online library or from the author.

SUPPLEMENTAL INFORMATION

Supplemental Information can be found online at https://doi.org/10.1016/j.xcrp.2020.100243.

ACKNOWLEDGMENTS

J.H.L. acknowledges the financial support of the National Natural Science Foundation of China (No. 21773195). G.Y. acknowledges the financial support of the National Natural Science Foundation of China (No. 21706129), W.Z. thanks the National Natural Science Foundation of China (No. 21576135) and the Jiangsu Natural Science Foundation for Distinguished Young Scholars (No. BK20170043) for support. X.Z. and L.C. acknowledge the financial support of the Fundamental Research Funds for the Central Universities of China (Grant No. XK1802-6 and 12060093063). Use of the Advanced Photon Source is supported by the U.S. Department of Energy, Office of Science and the Office of Basic Energy Sciences, under Contract DE-AC02-06CH11357. Q.L. acknowledges support from the Shanghai Science and Technology Committee (19010500400) and the 111 Project (D16002). H.F. acknowledges support from the National Natural Science Foundation of China (Grant No. 51701113) and Young Eastern Scholars (QD2016034). J.-L.L. acknowledges financial support from the Natural Sciences and Engineering Research Council of Canada Discovery Grant (GRPIN-2016-05494).

AUTHOR CONTRIBUTIONS

Y.-F.S. and B.H. conceived the study. Y.-F.S., Z.C., G.Y., J.L., and Y.-Q.Z. fabricated the samples. L.C. and X.Z. performed the first principles calculations. Y.-F.S., Y.Y., and Z.C. performed H_2-temperature programed reduction, Mott-Schottky measurement, optical measurements, and X-ray diffraction pattern. G.W. and H.Z. performed X-ray absorption measurements. Y.S., Z.C., Y.-Q.Z., Y.Y., H.F., and Q.L. performed the scanning electron microscopy and transmission electron microscopy. Y.-F.S., Y.Y., M.L., and G.Y. measured the catalytic performance of catalysts. Y.-F.S., B.H., Y.-Q.Z., Z.C., and X.Z. wrote the manuscript. All authors discussed the results and commented on the manuscript.

CellPress
OPEN ACCESS

Cell Reports
Physical Science
Article

DECLARATION OF INTERESTS

The authors declare no competing interests.

Received: October 22, 2019
Revised: September 17, 2020
Accepted: September 28, 2020
Published: October 28, 2020

REFERENCES

1. Tanaka, H., Taniguchi, M., Uenishi, M., Kajita, N., Tan, I., Nishihata, Y., Mizuki, J., Narita, K., Kimura, M., and Kaneko, K. (2006). Self-regenerating Rh- and Pt-based perovskite catalysts for automotive-emissions control. Angew. Chem. Int. Ed. *45*, 5998–6002.

2. Du, Z., Zhao, H., Yi, S., Xia, Q., Gong, Y., Zhang, Y., Cheng, X., Li, Y., Gu, L., and Świerczek, K. (2016). High-Performance Anode Material $Sr_2FeMo_{0.65}Ni_{0.35}O_{6-\delta}$ with In Situ Exsolved Nanoparticle Catalyst. ACS Nano *10*, 8660–8669.

3. Zhu, T., Troiani, H.E., Mogni, L.V., Han, M., and Barnett, S.A. (2018). Ni-Substituted $Sr(Ti,Fe)O_3$ SOFC Anodes: Achieving High Performance via Metal Alloy Nanoparticle Exsolution. Joule *2*, 478–496.

4. Adijanto, L., Balaji Padmanabhan, V., Küngas, R., Gorte, R.J., and Vohs, J.M. (2012). Transition metal-doped rare earth vanadates: a regenerable catalytic material for SOFC anodes. J. Mater. Chem. *22*, 11396.

5. Kwon, O., Kim, K., Joo, S., Jeong, H.Y., Shin, J., Han, J.W., Sengodan, S., and Kim, G. (2018). Self-assembled alloy nanoparticles in a layered double perovskite as a fuel oxidation catalyst for solid oxide fuel cells. J. Mater. Chem. A Mater. Energy Sustain. *6*, 15947–15953.

6. Jiang, S.P. (2012). Nanoscale and nano-structured electrodes of solid oxide fuel cells by infiltration: Advances and challenges. Int. J. Hydrogen Energy *37*, 449–470.

7. Chen, X., Ni, W., Wang, J., Zhong, Q., Han, M., and Zhu, T. (2018). Exploration of Co-Fe alloy precipitation and electrochemical behavior hysteresis using Lanthanum and Cobalt co-substituted $SrFeO_{3-\delta}$ SOFC anode. Electrochim. Acta *277*, 226–234.

8. Neagu, D., Papaioannou, E.I., Ramli, W.K.W., Miller, D.N., Murdoch, B.J., Ménard, H., Umar, A., Barlow, A.J., Cumpson, P.J., Irvine, J.T.S., and Metcalfe, I.S. (2017). Demonstration of chemistry at a point through restructuring and catalytic activation at anchored nanoparticles. Nat. Commun. *8*, 1855.

9. Neagu, D., Tsekouras, G., Miller, D.N., Ménard, H., and Irvine, J.T.S. (2013). In situ growth of nanoparticles through control of non-stoichiometry. Nat. Chem. *5*, 916–923.

10. Yang, C., Yang, Z., Jin, C., Xiao, G., Chen, F., and Han, M. (2012). Sulfur-tolerant redox-reversible anode material for direct hydrocarbon solid oxide fuel cells. Adv. Mater. *24*, 1439–1443.

11. Han, H., Park, J., Nam, S.Y., Kim, K.J., Choi, G.M., Parkin, S.S.P., Jang, H.M., and Irvine, J.T.S. (2019). Lattice strain-enhanced exsolution of nanoparticles in thin films. Nat. Commun. *10*, 1471.

12. Myung, J.H., Neagu, D., Miller, D.N., and Irvine, J.T.S. (2016). Switching on electrocatalytic activity in solid oxide cells. Nature *537*, 528–531.

13. Neagu, D., Oh, T.-S., Miller, D.N., Ménard, H., Bukhari, S.M., Gamble, S.R., Gorte, R.J., Vohs, J.M., and Irvine, J.T.S. (2015). Nano-socketed nickel particles with enhanced coking resistance grown in situ by redox exsolution. Nat. Commun. *6*, 8120.

14. Broggi, J., Terme, T., and Vanelle, P. (2014). Organic electron donors as powerful single-electron reducing agents in organic synthesis. Angew. Chem. Int. Ed. *53*, 384–413.

15. Prier, C.K., Rankic, D.A., and MacMillan, D.W.C. (2013). Visible light photoredox catalysis with transition metal complexes: applications in organic synthesis. Chem. Rev. *113*, 5322–5363.

16. Hwang, J., Rao, R.R., Giordano, L., Katayama, Y., Yu, Y., and Shao-Horn, Y. (2017). Perovskites in catalysis and electrocatalysis. Science *358*, 751–756.

17. Wheeler, G.P., and Choi, K.-S. (2017). Photoelectrochemical Properties and Stability of Nanoporous p-Type $LaFeO_3$ Photoelectrodes Prepared by Electrodeposition. ACS Energy Lett. *2*, 2378–2382.

18. Fleisch, T.H., Zajac, G.W., Schreiner, J.O., and Mains, G.J. (1986). An XPS study of the UV photoreduction of transition and noble metal oxides. Appl. Surf. Sci. *26*, 488–497.

19. Yang, G., Zhou, W., Liu, M., and Shao, Z. (2016). Enhancing Electrode Performance by Exsolved Nanoparticles: A Superior Cobalt-Free Perovskite Electrocatalyst for Solid Oxide Fuel Cells. ACS Appl. Mater. Interfaces *8*, 35308–35314.

20. Liu, S., Chuang, K.T., and Luo, J.-L. (2016). Double-layered perovskite anode within situ exsolution of a Co–Fe alloy to cogenerate ethylene and electricity in a proton-conducting ethane fuel cell. ACS Catal. *6*, 760–768.

21. Liu, S., Liu, Q., and Luo, J.-L. (2016). Highly stable and efficient catalyst with In Situ exsolved Fe–Ni alloy nanospheres socketed on an oxygen deficient perovskite for direct CO_2 electrolysis. ACS Catal. *6*, 6219–6228.

22. Sun, Y.-F., Li, J.-H., Zhang, Y.-Q., Hua, B., and Luo, J.-L. (2016). Bifunctional Catalyst of Core–Shell Nanoparticles Socketed on Oxygen-Deficient Layered Perovskite for Soot Combustion:In Situ Observation of Synergistic Dual Active Sites. ACS Catal. *6*, 2710–2714.

23. Boldrin, P., Ruiz-Trejo, E., Mermelstein, J., Bermúdez Menéndez, J.M., Ramı Rez Reina, T., and Brandon, N.P. (2016). Strategies for Carbon and Sulfur Tolerant Solid Oxide Fuel Cell Materials, Incorporating Lessons from Heterogeneous Catalysis. Chem. Rev. *116*, 13633–13684.

24. Li, J., Yu, Y., Yin, Y.-M., Zhou, N., and Ma, Z.-F. (2017). A novel high performance composite anode with in situ growth of Fe-Ni alloy nanoparticles for intermediate solid oxide fuel cells. Electrochim. Acta *235*, 317–322.

25. Qi, W., Ruan, C., Wu, G., Zhang, Y., Wang, Y., Xie, K., and Wu, Y. (2014). Reversibly in-situ anchoring copper nanocatalyst in perovskite titanate cathode for direct high-temperature steam electrolysis. Int. J. Hydrogen Energy *39*, 5485–5496.

26. Gao, Y., Wang, J., Lyu, Y.-Q., Lam, K., and Ciucci, F. (2017). In situ growth of Pt_3Ni nanoparticles on an A-site deficient perovskite with enhanced activity for the oxygen reduction reaction. J. Mater. Chem. A Mater. Energy Sustain. *5*, 6399–6404.

27. Liu, S., Liu, Q., and Luo, J.-L. (2016). CO_2-to-CO conversion on layered perovskite with in situ exsolved Co–Fe alloy nanoparticles: an active and stable cathode for solid oxide electrolysis cells. J. Mater. Chem. A Mater. Energy Sustain. *4*, 17521–17528.

28. Sun, Y., Li, J., Zeng, Y., Amirkhiz, B.S., Wang, M., Behnamian, Y., and Luo, J. (2015). A-site deficient perovskite: the parent for in situ exsolution of highly active, regenerable nano-particles as SOFC anodes. J. Mater. Chem. A Mater. Energy Sustain. *3*, 11048–11056.

29. Sun, Y.-F., Zhou, X.-W., Zeng, Y., Amirkhiz, B.S., Wang, M.-N., Zhang, L.-Z., Hua, B., Li, J., Li, J.-H., and Luo, J.-L. (2015). An ingenious Ni/Ce co-doped titanate based perovskite as a coking-tolerant anode material for direct hydrocarbon solid oxide fuel cells. J. Mater. Chem. A Mater. Energy Sustain. *3*, 22830–22838.

30. Kobsiriphat, W., Madsen, B.D., Wang, Y., Shah, M., Marks, L.D., and Barnett, S.A. (2010). Nickel- and ruthenium-doped lanthanum chromite anodes: effects of nanoscale metal precipitation on solid oxide fuel cell performance. J. Electrochem. Soc. *157*, B279.

31. Gao, Y., Chen, D., Saccoccio, M., Lu, Z., and Ciucci, F. (2016). From material design to mechanism study: Nanoscale Ni exsolution on a highly active A-site deficient anode material

for solid oxide fuel cells. Nano Energy *27*, 499–508.

32. Hua, B., Li, M., Sun, Y.-F., Zhang, Y.-Q., Yan, N., Chen, J., Thundat, T., Li, J., and Luo, J.-L. (2017). A coupling for success: Controlled growth of Co/CoOx nanoshoots on perovskite mesoporous nanofibres as high-performance trifunctional electrocatalysts in alkaline condition. Nano Energy *32*, 247–254.

33. Zhu, Y., Zhou, W., Ran, R., Chen, Y., Shao, Z., and Liu, M. (2016). Promotion of Oxygen Reduction by Exsolved Silver Nanoparticles on a Perovskite Scaffold for Low-Temperature Solid Oxide Fuel Cells. Nano Lett. *16*, 512–518.

34. Sun, Y.-F., Zhang, Y.-Q., Chen, J., Li, J.-H., Zhu, Y.-T., Zeng, Y.-M., Amirkhiz, B.S., Li, J., Hua, B., and Luo, J.-L. (2016). New Opportunity for in Situ Exsolution of Metallic Nanoparticles on Perovskite Parent. Nano Lett. *16*, 5303–5309.

35. Sun, Y.-F., Li, J.-H., Cui, L., Hua, B., Cui, S.-H., Li, J., and Luo, J.-L. (2015). A-site-deficiency facilitated in situ growth of bimetallic Ni-Fe nano-alloys: a novel coking-tolerant fuel cell anode catalyst. Nanoscale *7*, 11173–11181.

36. Ye, L., Zhang, M., Huang, P., Guo, G., Hong, M., Li, C., Irvine, J.T., and Xie, K. (2017). Enhancing CO_2 electrolysis through synergistic control of non-stoichiometry and doping to tune cathode surface structures. Nat. Commun. *8*, 14785.

37. Irvine, J.T.S., Neagu, D., Verbraeken, M.C., Chatzichristodoulou, C., Graves, C., and Mogensen, M.B. (2016). Evolution of the electrochemical interface in high-temperature fuel cells and electrolysers. Nat. Energy *1*, 15014.

38. Wei, H.S., Xie, K., Zhang, J., Zhang, Y., Wang, Y., Qin, Y.Q., Cui, J.W., Yan, J., and Wu, Y.C. (2014). In situ growth of Ni_xCu_{1-x} alloy nanocatalysts on redox-reversible rutile (Nb, Ti)O_4 towards high-temperature carbon dioxide electrolysis. Sci. Rep. *4*, 11.

39. Sun, Y.-F., Li, J.-H., Wang, M.-N., Hua, B., Li, J., and Luo, J.-L. (2015). A-site deficient chromite perovskite with in situ exsolution of nano-Fe: a promising bi-functional catalyst bridging the growth of CNTs and SOFCs. J. Mater. Chem. A Mater. Energy Sustain. *3*, 14625–14630.

40. Kwon, O., Sengodan, S., Kim, K., Kim, G., Jeong, H.Y., Shin, J., Ju, Y.-W., Han, J.W., and Kim, G. (2017). Exsolution trends and co-segregation aspects of self-grown catalyst nanoparticles in perovskites. Nat. Commun. *8*, 15967.

41. Jardiel, T., Caldes, M.T., Moser, F., Hamon, J., Gauthier, G., and Joubert, O. (2010). New SOFC electrode materials: The Ni-substituted LSCM-based compounds $(La_{0.75}Sr_{0.25})(Cr_{0.5}Mn_{0.5-x}Ni_x)O_{3-\delta}$ and $(La_{0.75}Sr_{0.25})(Cr_{0.5-x}Ni_xMn_{0.5})O_{3-\delta}$. Solid State Ion. *181*, 894–901.

42. Zhang, J., Xie, K., Zhang, Y., Yang, L., Wu, G., Qin, Q., Li, Y., and Wu, Y. (2014). Composite titanate cathode decorated with heterogeneous electrocatalytic sites towards efficient carbon dioxide electrolysis. RSC Advances *4*, 22697–22709.

43. Zhou, J., Shin, T.H., Ni, C.S., Chen, G., Wu, K., Cheng, Y.H., and Irvine, J.T.S. (2016). In Situ Growth of Nanoparticles in Layered Perovskite $La_{0.8}Sr_{1.2}Fe_{0.9}Co_{0.1}O_{4-\delta}$ as an Active and Stable Electrode for Symmetrical Solid Oxide Fuel Cells. Chem. Mater. *28*, 2981–2993.

44. Gan, L., Ye, L., Tao, S., and Xie, K. (2016). Titanate cathodes with enhanced electrical properties achieved via growing surface Ni particles toward efficient carbon dioxide electrolysis. Phys. Chem. Chem. Phys. *18*, 3137–3143.

45. Yang, L., Xie, K., Xu, S., Wu, T., Zhou, Q., Xie, T., and Wu, Y. (2014). Redox-reversible niobium-doped strontium titanate decorated with in situ grown nickel nanocatalyst for high-temperature direct steam electrolysis. Dalton Trans. *43*, 14147–14157.

46. Arrive, C., Delahaye, T., Joubert, O., and Gauthier, G. (2013). Exsolution of nickel nanoparticles at the surface of a conducting titanate as potential hydrogen electrode material for solid oxide electrochemical cells. J. Power Sources *223*, 341–348.

47. Park, B.H., and Choi, G.M. (2015). Effect of anode firing on the performance of lanthanum and nickel co-doped $SrTiO_3$ $(La_{0.2}Sr_{0.8}Ti_{0.9}Ni_{0.1}O_{3-\delta})$ anode of solid oxide fuel cell. J. Power Sources *293*, 684–691.

48. Wang, Y., Liu, T., Li, M., Xia, C., Zhou, B., and Chen, F. (2016). Exsolved Fe-Ni nano-particles from $Sr_2Fe_{1.3}Ni_{0.2}Mo_{0.5}O_6$ perovskite oxide as a cathode for solid oxide steam electrolysis cells. J. Mater. Chem. A Mater. Energy Sustain. *4*, 14163–14169.

49. Lan, R., Cowin, P.I., Sengodan, S., and Tao, S. (2016). A perovskite oxide with high conductivities in both air and reducing atmosphere for use as electrode for solid oxide fuel cells. Sci. Rep. *6*, 31839.

50. Yang, C.H., Li, J., Lin, Y., Liu, J., Chen, F.L., and Liu, M.L. (2015). In situ fabrication of CoFe alloy nanoparticles structured $(Pr_{0.4}Sr_{0.6})_3(Fe_{0.85}Nb_{0.15})_2O_7$ ceramic anode for direct hydrocarbon solid oxide fuel cells. Nano Energy *11*, 704–710.

51. Bierschenk, D.M., Potter-Nelson, E., Hoel, C., Liao, Y.G., Marks, L., Poeppelmeier, K.R., and Barnett, S.A. (2011). Pd-substituted (La,Sr)$CrO_{3-\delta}$-$Ce_{0.9}Gd_{0.1}O_{2-\delta}$ solid oxide fuel cell anodes exhibiting regenerative behavior. J. Power Sources *196*, 3089–3094.

52. Caudle, M.T., and Pecoraro, V.L. (2000). Mechanism for the reduction of the mixed-valent $Mn^{III}Mn^{IV}$[2-OHsalpn]$_2^+$ complex by tertiary amines. Inorg. Chem. *39*, 5831–5837.

53. Xu, X., Randorn, C., Efstathiou, P., and Irvine, J.T.S. (2012). A red metallic oxide photocatalyst. Nat. Mater. *11*, 595–598.

54. Chen, S., and Wang, L.-W. (2012). Thermodynamic Oxidation and Reduction Potentials of Photocatalytic Semiconductors in Aqueous Solution. Chem. Mater. *24*, 3659–3666.

55. Klimov, V.I., Ivanov, S.A., Nanda, J., Achermann, M., Bezel, I., McGuire, J.A., and Piryatinski, A. (2007). Single-exciton optical gain in semiconductor nanocrystals. Nature *447*, 441–446.

56. Roth, H.G., Romero, N.A., and Nicewicz, D.A. (2016). Experimental and calculated electrochemical potentials of common organic molecules for applications to single-electron redox chemistry. Synlett *27*, 714–723.

57. Cossy, J., and Belotti, D. (2006). Generation of ketyl radical anions by photoinduced electron transfer (PET) between ketones and amines. Synthetic applications. Tetrahedron *62*, 6459–6470.

58. Steiger, P., Delmelle, R., Foppiano, D., Holzer, L., Heel, A., Nachtegaal, M., Kröcher, O., and Ferri, D. (2017). Structural Reversibility and Nickel Particle stability in Lanthanum Iron Nickel Perovskite-Type Catalysts. ChemSusChem *10*, 2505–2517.

59. Subbaraman, R., Tripkovic, D., Chang, K.-C., Strmcnik, D., Paulikas, A.P., Hirunsit, P., Chan, M., Greeley, J., Stamenkovic, V., and Markovic, N.M. (2012). Trends in activity for the water electrolyser reactions on 3d M(Ni,Co,Fe,Mn) hydr(oxy)oxide catalysts. Nat. Mater. *11*, 550–557.

60. Wang, J., Zhong, H.X., Qin, Y.L., and Zhang, X.B. (2013). An efficient three-dimensional oxygen evolution electrode. Angew. Chem. Int. Ed. *52*, 5248–5253.

61. Zhu, Y., Zhou, W., Chen, Z.-G., Chen, Y., Su, C., Tadé, M.O., and Shao, Z. (2015). $SrNb_{(0.1)}Co_{(0.7)}Fe_{(0.2)}O_{(3-\delta)}$ perovskite as a next-generation electrocatalyst for oxygen evolution in alkaline solution. Angew. Chem. Int. Ed. *54*, 3897–3901.